Metals

CrossMark

Microstructural evolution during hot shear deformation of an extruded fine-grained Mg–Gd–Y–Zr alloy

R. Alizadeh[1], R. Mahmudi[1,*], A. H. W. Ngan[2], and T. G. Langdon[3]

[1] *School of Metallurgical and Materials Engineering, College of Engineering, University of Tehran, Tehran, Iran*

[2] *Department of Mechanical Engineering, The University of Hong Kong, Pokfulam Road, Pok Fu Lam, Hong Kong*

[3] *Materials Research Group, Faculty of Engineering and the Environment, University of Southampton, Southampton SO17 1BJ, UK*

ABSTRACT

Mg–Gd–Y–Zr alloys are among recently developed Mg alloys having superior mechanical properties at elevated temperatures. Dynamic recrystallization (DRX) and rare earth-rich particles play important roles in enhancing the high-temperature strength of these alloys. Accordingly, the microstructural evolution of a fine-grained extruded Mg–5Gd–4Y–0.4Zr alloy was investigated after hot shear deformation in the temperature range of 350–450 °C using the shear punch testing (SPT) method. The results reveal the occurrence of partial dynamic recrystallization at the grain boundaries at 350 °C while the fraction of DRX grains increases with increasing deformation temperature. A fully recrystallized microstructure was achieved after SPT at 450 °C. The Gd-rich and Y-rich cuboid particles, having typical sizes in the range of ~ 50 nm to ~ 3 μm, show excellent stability and compatibility after hot shear deformation, and these particles enhance the high-temperature strength during hot deformation at elevated temperatures. The textural evolution, examined using electron backscattered diffraction, revealed a non-fibrous basal DRX texture after SPT which is different from the conventional deformation texture.

Introduction

Magnesium alloys based on the Mg–Al–Zn system suffer from poor mechanical properties at elevated temperatures, and accordingly, attempts have been made to improve these properties through the addition of alloying elements. For example, there are reports that rare earth (RE) elements can greatly improve the microstructural stability of Mg alloys at high temperatures [1–4]. Among the newly developed Mg–RE-based alloys are Mg–Gd–Y alloys which exhibit superior strength [5–7] and creep resistance [8, 9]. In addition, these alloys show the potential for superplasticity in both the fine-grained [10, 11] and nano-grained [12, 13] states. These exceptional properties originate primarily from the influence of RE elements on the restoration processes and the textural evolution of Mg alloys at elevated temperatures [14, 15] and also from the presence of RE-rich precipitates having superior thermal stability

Address correspondence to E-mail: mahmudi@ut.ac.ir

Springer

[4]. These results suggest that it would be valuable to investigate the hot deformation of Mg–Gd–Y alloys to obtain a better understanding of the dominant flow mechanisms at these high temperatures.

Some limited research has been conducted recently on the hot deformation of Mg–Gd–Y alloys, but these investigations have generally used constitutive analyses and/or processing maps so that only limited information is available on microstructural evolution at elevated temperatures. Generally, discontinuous dynamic recrystallization (DDRX) has been invoked as the most important microstructural restoration process in Mg–Gd–Y alloys at elevated temperatures and a summary of the experimental conditions used in these reports is given in Table 1 where all data relate to hot compression [16–20]. The processing condition, the resultant grain size where reported, the testing temperature and the strain rate ranges are all listed in Table 1, and inspection shows that most reports relate to alloys in the cast condition and there is only one investigation of an Mg–Gd–Y alloy in the extruded condition [19]. Furthermore, there have been no investigations using other deformation procedures such as shear testing. Thus, despite the important role of RE-rich particles in enhancing the high-temperature strength of Mg–RE alloys, relatively little attention has been devoted to the microstructural evolution and the role of these particles during hot deformation. Furthermore, there are at present no investigations of the textural evolution of Mg–Gd–Y alloys after hot deformation.

While hot compression testing is the most common procedure for hot deformation studies, investigations of hot deformation of metallic alloys by localized testing techniques are of significant interest. Recently, shear punch testing (SPT) needing very small thin samples was successfully used for evaluating the hot deformation characteristics of Mg–Li alloys [21, 22] and Mg–Gd–Zn alloys [23] through constitutive analysis. Thus, the present investigation was initiated to investigate the microstructural and textural evolution of an Mg–5Gd–4Y–0.4Zr alloy during hot shear deformation using SPT at different temperatures and strain rates and to determine the underlying restoration processes and also the role of the RE-rich precipitates in enhancing the high-temperature behavior of this alloy.

Experimental material and procedures

An Mg–5 wt% Gd–4 wt% Y–0.4 wt% Zr alloy was used for this investigation with the alloy prepared from high-purity Mg and Mg–30Gd, Mg–30Y and Mg–30Zr master alloys. Details of the melting and extrusion processes were described earlier [14, 24], but, briefly, the required metal was melted in an electric resistance furnace under a protective flux cover, poured into a steel die preheated to 300 °C using a tilt-casting system to minimize casting defects and melt turbulence and then extruding at 400 °C with an extrusion ratio of 19:1. The hot shear deformation was assessed using SPT, and again the details were given earlier [25]. Sample preparation for SPT involved cutting thin disks of $\sim 0.90 \pm 0.05$ mm thickness perpendicular to the extrusion direction (ED) using electro-discharge machining (EDM) and then reducing the thickness by soft grinding to $\sim 0.70 \pm 0.05$ mm to remove any surface roughness. The prepared samples were placed within an SPT fixture having a 2.957-mm-diameter flat cylindrical punch and a 3.044-mm-diameter receiving hole. The load required to deform the sample, F, was measured

Table 1 Summary of the literature data on the hot deformation of Mg–Gd–Y alloys

Alloy	Initial condition		Test conditions		References
	Process	Grain size (µm)	Temperature (°C)	Strain rate (s^{-1})	
Mg–7Gd–5Y–1.2 N–1Zr	As-cast	–	300–450	0.002–1	[16]
Mg–9.3Gd–2.9Y–0.35Zr	Cast + homogenized	–	300–450	0.001–1	[17]
Mg–6.85Gd–4.52Y–1.15Nd–0.55Zr	Cast + homogenized	200	350–530	0.005–5	[18]
Mg–8.90Gd–5.11Y–3.10Zn–0.47Zr	Extrusion	–	300–500	0.001–1	[19]
Mg–11Gd–2Y–1Zn–1Zr	Cast + homogenized	–	350–480	0.001–0.5	[20]

automatically as a function of the punch displacement, and the data were recorded using appropriate software to determine the shear stress, τ, on the tested material based on the following relationship [26]

$$\tau = \frac{F}{\pi D t} \qquad (1)$$

where t is the specimen thickness and D is the average of the punch and die hole diameters. The SPT curves were plotted as shear stress against punch displacement normalized to the initial thickness. The SPT was performed at temperatures of 350, 400 and 450 °C under two shear strain rates, $\dot{\gamma}$, of 3.3×10^{-2} and 2.7×10^{-1} s^{-1} using a screw-driven MTS testing system equipped with a three-zone split furnace.

The microstructures of the samples, both before and after SPT, were characterized using a Hitachi S-3400N variable pressure scanning electron microscope (SEM) and a Hitachi S-4800 field emission gun scanning electron microscope (FEGSEM) after etching the samples in an acetic picral solution. The crystal structure and chemical composition of the precipitates were examined using an FEI Tecnai G2 20 S-TWIN scanning transmission electron microscope (STEM) with a maximum operating voltage of 200 kV. After grinding to $\sim$100 μm thickness, the TEM disks were further reduced to $\sim$20 μm with a dimpler machine and the TEM samples were finally prepared by ion beam milling (IBM). Electron backscattered diffraction (EBSD) was used to study the orientation maps and texture evolution. The specimen preparation for EBSD involved grinding with SiC paper and diamond paste polishing followed by vibratory polishing with an alcohol-based alumina solution.

Experimental results

Microstructure before SPT

Representative SEM micrographs at two different magnifications are shown in Fig. 1 corresponding to the plane perpendicular to ED. It is apparent that the microstructure after hot extrusion at 400 °C consists of fine equiaxed grains with an average size of $\sim$4.6 $\pm$ 0.2 μm indicating the occurrence of dynamic recrystallization (DRX) and with small cuboid particles which appear to be rich in RE located both at the grain boundaries and within the grains. The
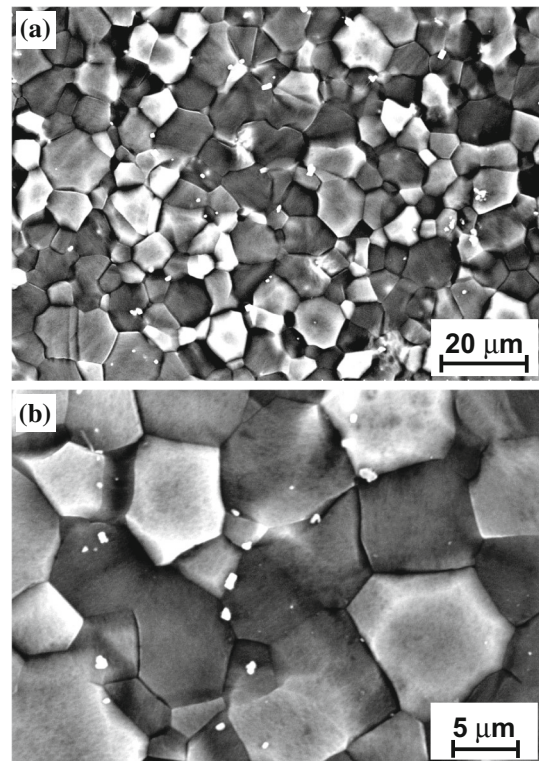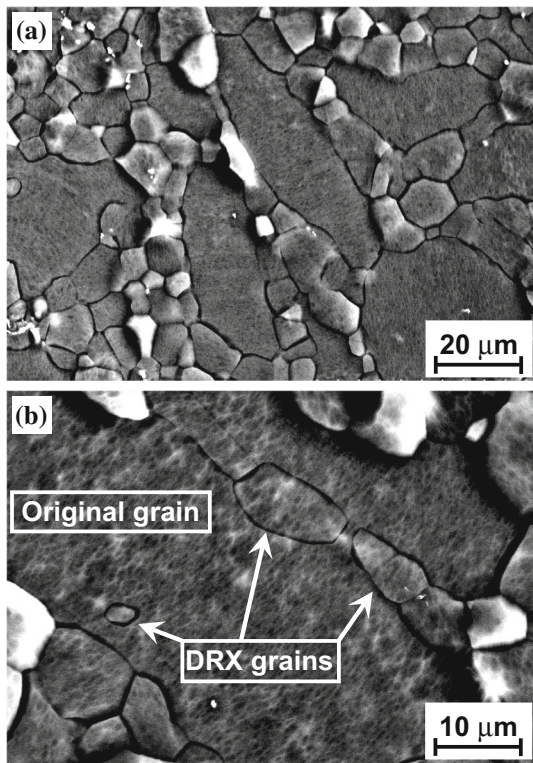

Figure 1 SEM micrographs of the alloy in the ED showing **a** the grain structure and **b** the distribution of the second-phase particles.
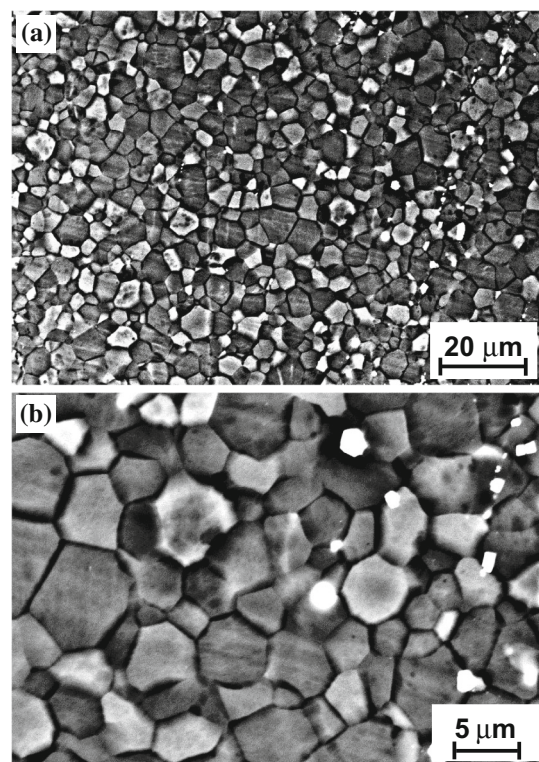
Figure 2 SEM micrographs of the alloy in the TD showing **a** the grain structure and **b** the distribution of particles.
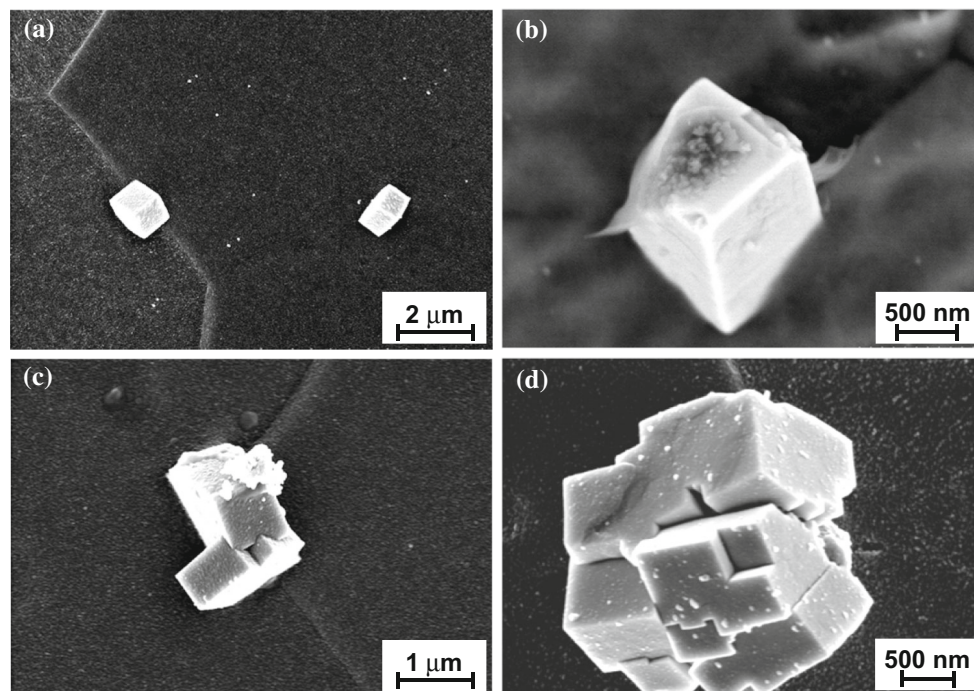
Figure 3 SEM micrographs of the alloy, extruded with low ratio of 8:1, showing **a** the necklace structure and **b** formation of new DRX grains at the original grain boundaries.

microstructure in the transverse direction (TD) on the plane parallel to ED is shown in Fig. 2 at two different magnifications. These micrographs show there are no elongated grains in either the ED or TD and it is reasonable to conclude that the DRX is complete. Regarding the DRX mechanism of the alloy during the extrusion process, it was shown earlier [14] that new DRX grains form at the original grain boundaries during hot deformation, and therefore, it was concluded that the DDRX can be considered as the main mechanism of recrystallization. The microstructure of the Mg–5Gd–4Y–0.4Zr alloy, extruded with lower extrusion ratio of 8:1, is shown in Fig. 3 to better explore the formation of DRX grains during deformation. As can be observed in this figure, a necklace structure was developed after the extrusion process, which can be considered as an indication of the occurrence of the DDRX mechanism. The formation of newly developed DRX grains at the original grain boundaries is shown in Fig. 3b.

High-magnification FEGSEM micrographs of the particles are shown in Fig. 4 which confirms that the RE-rich particles are present in the form of small cuboidal shapes. In Fig. 4a, there are two cuboidal particles, one formed at the grain boundary and the

Figure 4 FEGSEM micrographs of the alloy showing the positions, shapes and sizes of some representative *cuboid* particles.

other within a grain. A cuboid particle embedded at a grain boundary is shown in Fig. 4b at a higher magnification. In addition to these isolated particles, some agglomerated particles were also present as shown in Fig. 4c, d. Comprehensive microstructural characterization showed that the sizes of these cuboid particles varied within the range of ∼50 nm up to ∼3 μm.

The chemical compositions of the cuboidal particles were checked qualitatively by SEM using an energy-dispersive X-ray spectroscopy (EDS) line scan, and the results are shown in Fig. 5. These results provide a clear demonstration that the particles are rich in Gd and Y. Elemental maps for Mg, Gd and Y are also shown in Fig. 6 for the agglomerated particles in Fig. 4d. In accordance with the results in Fig. 5, the agglomerated cuboidal particles are rich in Gd and Y while also containing small amounts of Mg. In order to study the chemical composition of these particles quantitatively, a TEM–EDS analysis was performed on some selected particles and a typical result is summarized in Fig. 7. The results indicate that the cuboidal particle in Fig. 7a is rich in Gd and Y and, according to the atomic concentration values, the chemical composition is close to $Mg_2(Gd, Y)$. The crystal structure of the precipitate was also studied through selected area electron diffraction (SAED), and the results are shown in Fig. 7b where the pattern was indexed as face-centered cubic (fcc) with a lattice parameter of ∼0.54 ± 0.02 nm. Similar fcc crystal structures with lattice parameters in the range ∼0.54 to 0.56 nm were reported earlier for cuboid Mg-RE precipitates [14, 27–31].

SPT results

Shear punch test curves are shown in Fig. 8 for temperatures of 350, 400 and 450 °C under shear strain rates of (a) 3.3×10^{-2} and (b) 2.7×10^{-1} s^{-1}. It is evident that the flow behavior depends strongly on both temperature and strain rate, thereby suggesting that different deformation mechanisms may operate at different temperatures and strain rates. Thus, the microstructures of the samples will be affected by these different mechanisms after deformation under
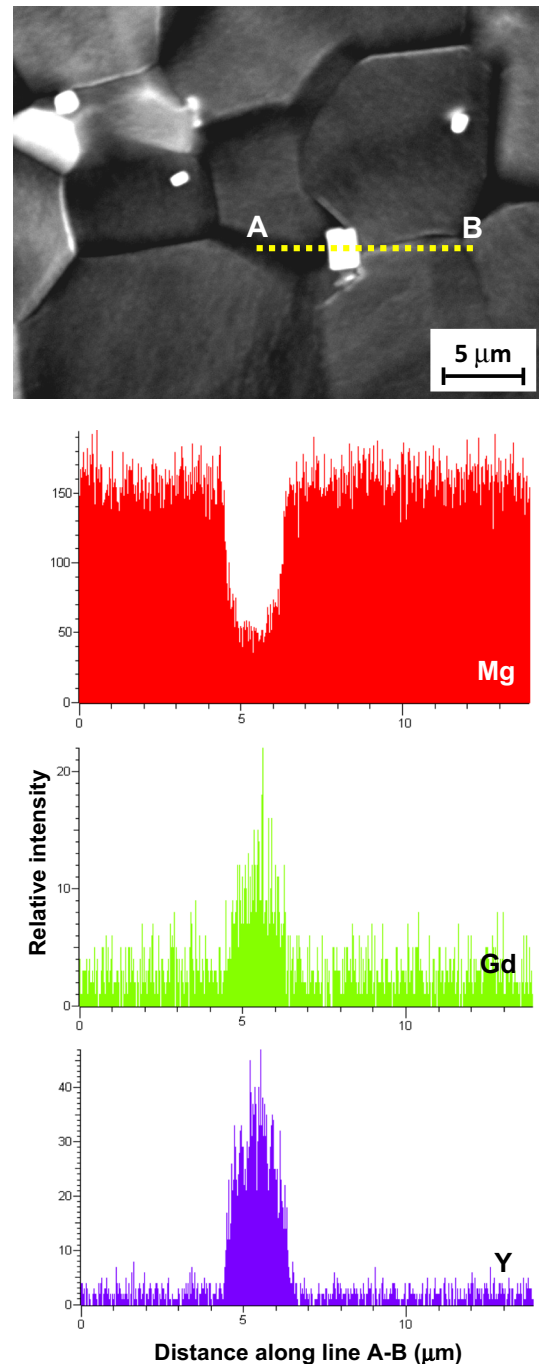
Figure 5 SEM–EDS line scan along *A–B* showing the results for Mg, Gd and Y.

different conditions, and accordingly, it is necessary to examine the microstructural evolution in more detail.
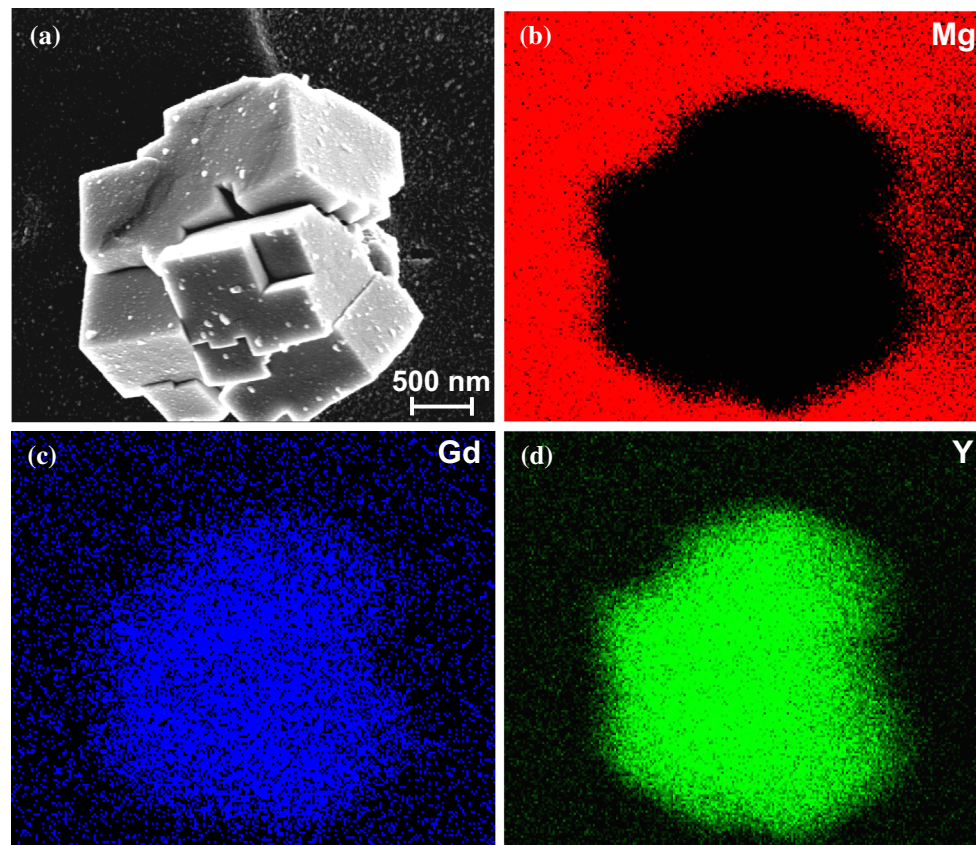
Figure 6 **a** SEM micrograph of agglomerated *cuboid* particles and the corresponding elemental maps for **b** Mg, **c** Gd and **d** Y.

Microstructural and textural evolution after SPT

The microstructural evolution after hot shear deformation was examined by inspecting the cross-section of the hot deformed samples using SEM and FEG-SEM. A schematic illustration of the SPT sample showing different areas of the sample both before and after deformation together with a low-magnification SEM micrograph of a sample after SPT is given in Fig. 9. Three important areas may be identified on each sample: deformation (1), the die (2) and under the punch (3). Since almost all of the shear deformation occurs within the deformation area, most of the microstructural characterizations were focused on this area. However, for a direct comparison with the microstructure of the material experiencing a high temperature but no shear deformation, the microstructure was also examined in the die area. The microstructural evolution was also examined

under the punch, but these results were essentially identical to those obtained in the die area.

The microstructures of the material after SPT at 350 °C under a shear strain rate of $2.7 \times 10^{-1}\ s^{-1}$ are shown in Fig. 10 where (a–d) are within the deformation area and (e, f) are in the die area. It is clear that the grains are deformed and elongated in the shear direction and the grain boundaries are thickened in the deformation area, whereas by moving from the deformation area toward the die area the grains reasonably retain their original un-deformed shapes and the grain boundaries are thinner. These features indicate that partial DRX occurs at the original grain boundaries at 350 °C, but the deformed grains retain their elongated shapes. By increasing the deformation temperature to 400 °C, the microstructure becomes more uniform in the deformation area in Fig. 11a–c and there are almost no elongated grains except in some small areas as within the area delineated by the broken line in Fig. 11c.
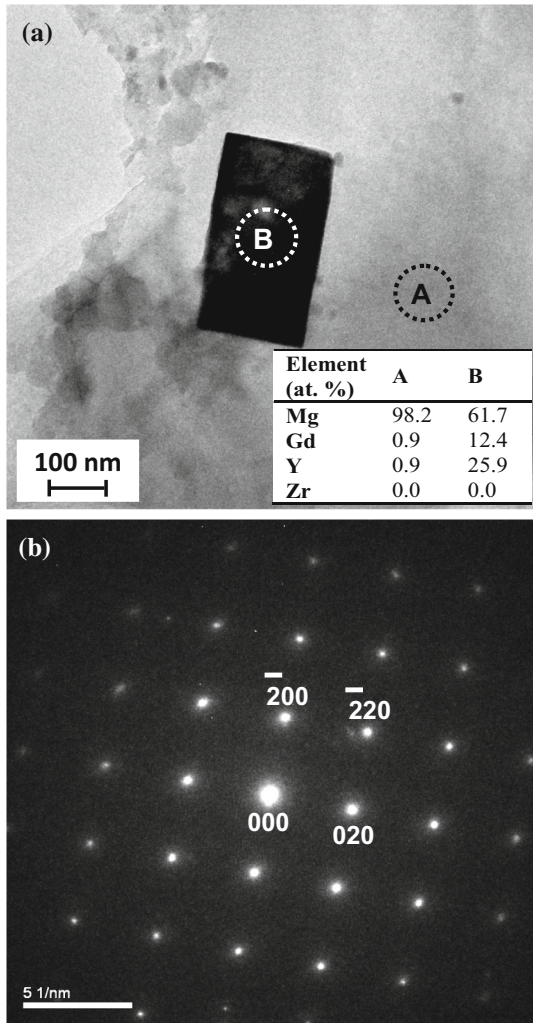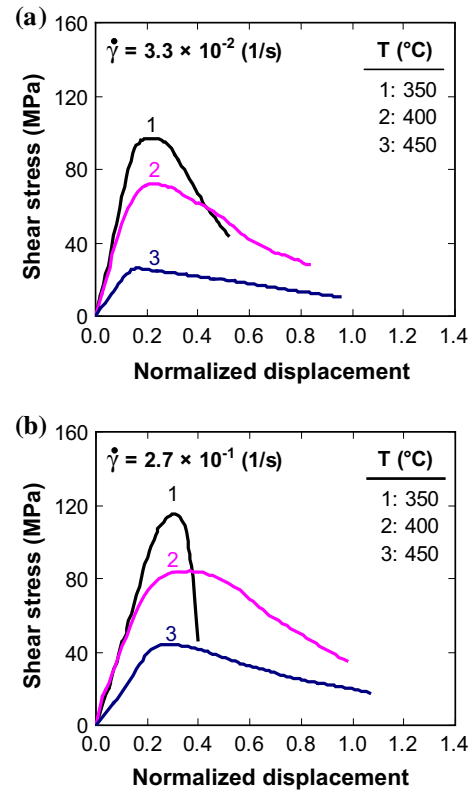
Figure 7 **a** TEM micrograph and **b** corresponding SAED pattern of one of the *cuboid* particles with zone axis parallel to [001].

Figure 8 SPT curves at different temperatures for shear strain rates of **a** 3.3×10^{-2} s^{-1} and **b** 2.7×10^{-1} s^{-1}.

This indicates that increasing the temperature form 350 to 400 °C leads to a replacement of the deformed grains by newly formed DRX grains which are nucleated at the grain boundaries of the original grains.

The microstructures of the material after SPT deformation at 450 °C under two shear strain rates of 3.3×10^{-2} and 2.7×10^{-1} s^{-1} are shown in Figs. 12 and 13, respectively, where (a–c) relate to the deformation area and (d) is for the die area. It is apparent that fine equiaxed grains are formed in the deformation area and these grains are finer than in the die area. Also, in contrast to the lower deformation temperature, no elongated grains are found in the deformation area which indicates the occurrence of complete DRX at 450 °C. However, the grain sizes are relatively larger than those obtained at 400 and

350 °C. Concerning the effect of strain rate, according to the microstructures of the alloy shown in Figs. 12 and 13 for respective shear strain rates of 3.3×10^{-2} and 2.7×10^{-1} s^{-1}, it is observed that fine equiaxed grains are formed at 450 °C irrespective of the applied strain rates. Additionally, no distinct differences were detected between the grain sizes of the material in the deformation areas of the samples deformed under different strain rates.

Since RE-rich particles play an important role in enhancing superior strength of Mg–Gd–Y alloys at elevated temperatures, it is of interest to examine the morphologies of these particles after hot shear deformation. Accordingly, the morphology of the cuboid particles after hot shear deformation at 400 °C under shear strain rates of 3.3×10^{-2} and 2.7×10^{-1} s^{-1} was examined at high magnifications through FEGSEM and the results are presented in Fig. 14 showing the shape, size and distribution of these particles. All micrographs were taken in the deformation area. Inspection shows that the Gd- and Y-rich cuboid particles do not undergo any significant change in shape, fragmentation or deformation while the magnesium matrix is severely deformed

(a)

(b)
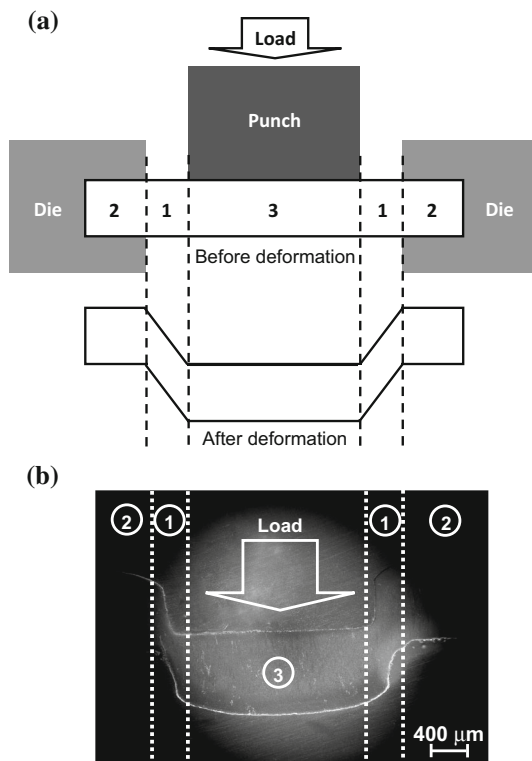
Figure 9 a Schematic illustration of a sample before and after SPT and **b** a low-magnification SEM micrograph of a sample after SPT showing areas corresponding to deformation (*1*), the die (*2*) and under the punch (*3*).

within the deformation area. Thus, these particles retain their original shapes. Furthermore, no cracks or voids were detected around these particles even at high magnifications. All of these features demonstrate the excellent thermal stability of these particles and also their compatibility with the Mg matrix during deformation, where both of these factors will enhance the high-temperature strength properties of Mg–Gd–Y alloys. An additional important point is that no newly formed fine grains were observed around any of the cuboid particles.

In addition to the shape and size of the newly formed grains due to the DRX during hot shear deformation, the crystallographic orientations of these grains are important because it may affect the high-temperature mechanical properties of the material. Accordingly, the orientation maps of the grains after SPT at 450 °C were obtained by EBSD and the results are shown in Fig. 15. It is readily apparent from Fig. 15a and b that the grains are equiaxed in the shear deformation area and there are

no elongated grains. Therefore, it is concluded that complete DRX occurs during hot shear deformation of the alloy at 450 °C. The corresponding pole figures are shown in Fig. 15c for the (0001) and (10$\bar{1}$0) planes, and it is apparent that there is a relatively strong basal texture with a maximum intensity of 7.8 MRD (multiplies of random distribution). A comparison of this texture with the initial texture before SPT is presented in the next section.

Discussion

Microstructural evolution after hot shear deformation

A comparison of Figs. 10, 11, 12 and 13 demonstrates that, although there is some DRX in the Mg–5Gd–4Y–0.4Zr alloy even at a temperature of 350 °C, complete DRX occurs only at 450 °C. The microstructure of the material after hot shear deformation at 350 °C consisted of deformed grains which are surrounded by a typical necklace-like structure which is produced by the DRX. Thus, the DRX occurs only locally at the grain boundaries of the original grains at 350 °C, and therefore, very fine grains are formed at the grain boundaries while the original grains remain deformed and elongated in the direction of shear deformation. These features are consistent with the discontinuous dynamic recrystallization mechanism which is generally considered the dominant recrystallization mechanism in Mg alloys. By increasing the temperature to 400 °C, DRX occurs more readily and leads to a thickening of the bands of newly formed DRX grains toward the centers of the original grains. Except in some small areas, almost all of the microstructures are recrystallized at 400 °C. Complete recrystallization occurs by increasing the deformation temperature to 450 °C where fully recrystallized equiaxed grains are formed within the deformation area.

In comparison with earlier studies of Mg–Gd–Y alloys, it is noted that the present results are consistent with those reported for other similar alloys [16–20]. For example, it was reported that grain growth occurs at 500 °C in an extruded Mg–8.90Gd–5.11Y–3.10Zn–0.47Zr alloy, but fine DRX grains form at 400 °C [19]. Also, the temperature range of 375–450 °C was suggested earlier as the appropriate temperature range for DRX of an as-cast and
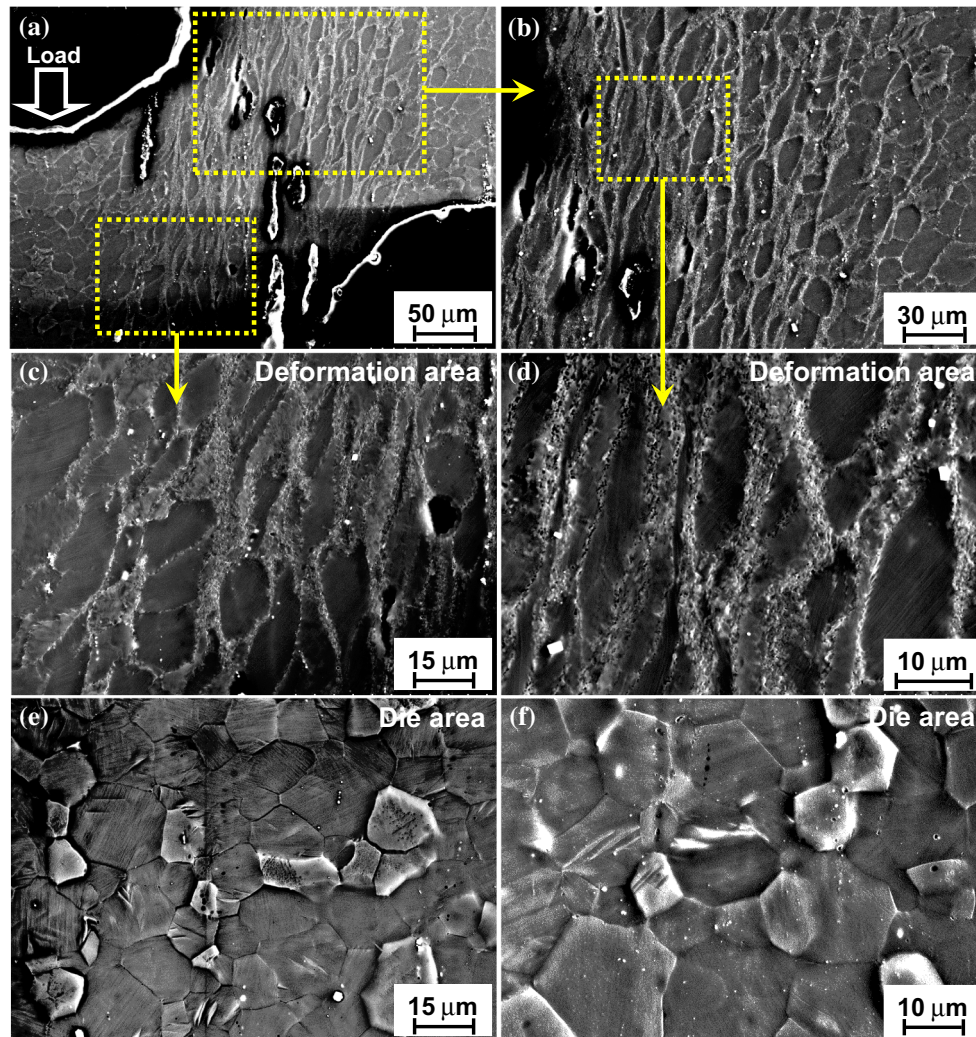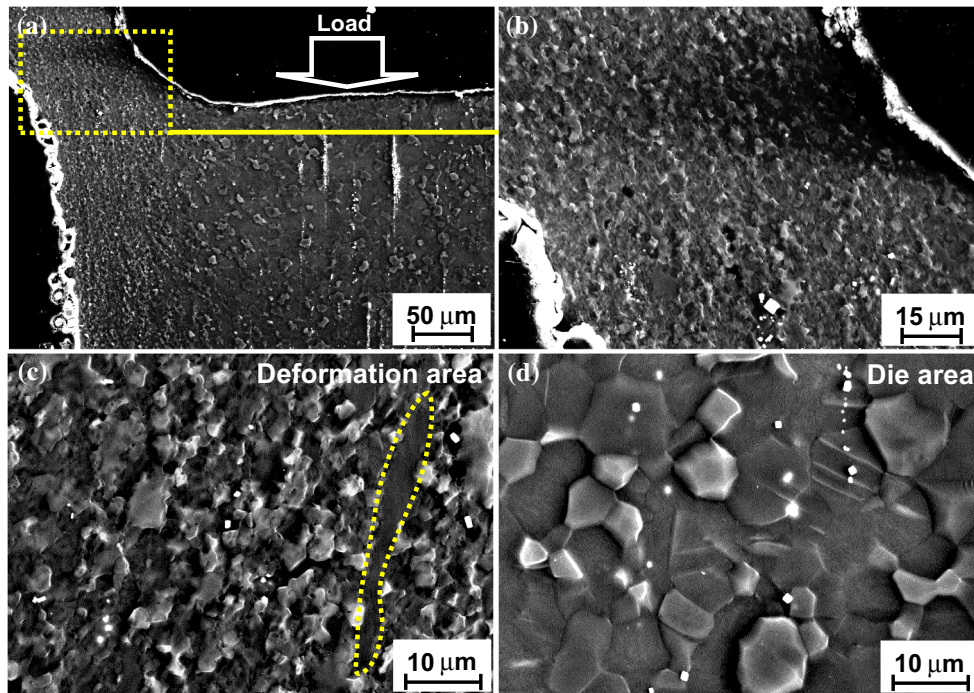
Figure 10 SEM micrographs of the material after SPT at 350 °C under a strain rate of 2.7 × 10^{-1} s^{-1}: **a, b** deformation area and adjacent regions, **c, d** deformation area and **e, f** die area.

homogenized Mg–9.3Gd–2.9Y–0.3Zr alloy [17]. A microstructural characterization of a hot compressed as-cast binary Mg–1.5Gd alloy at 400 °C also revealed the local occurrence of DRX at the original grain boundaries and the development of necklace-like structures [32]. However, static annealing of these samples at 450 °C for 1 h resulted in fully recrystallized microstructures [33].

It should be noted that the hot deformation behavior of the Mg–Gd–Y–Zr alloy in this investigation is different from conventional Mg alloys without

the presence of RE elements. Although the DRX is the dominant recrystallization mechanism in both RE-containing and RE-free magnesium alloys, there are some fundamental differences between their recrystallization behaviors. These differences are attributed to the role of the RE elements in delineating the onset temperature of recrystallization, the amount of stored energy [32] and the crystallographic texture of the newly formed DRX grains [14, 33]. As an example, while DRX occurs at grain boundaries of an AZ31 alloy at 300 °C, there was no evidence for the
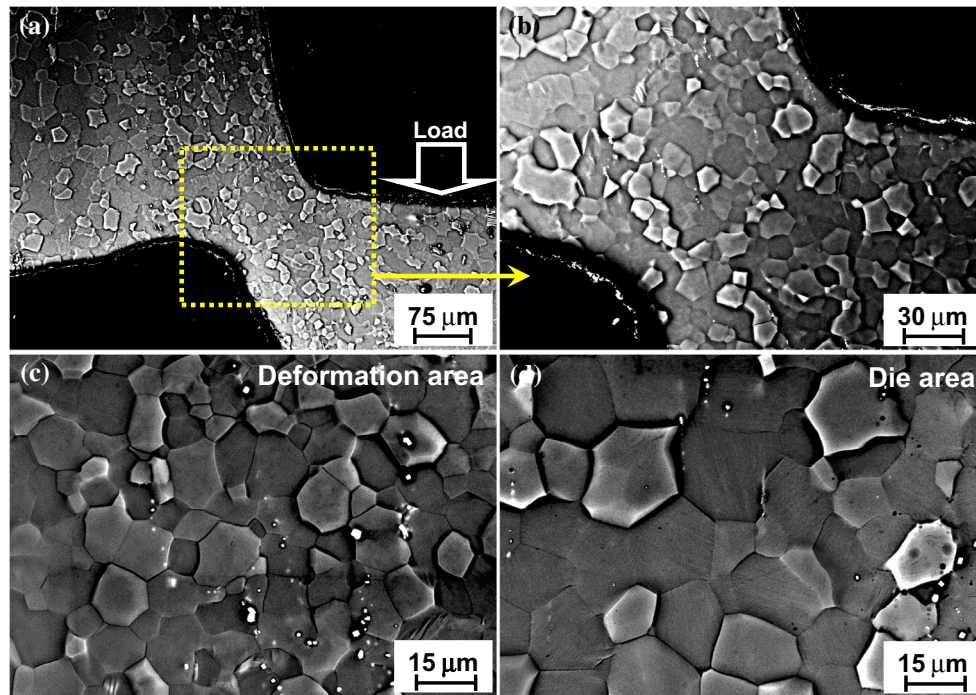
Figure 11 SEM micrographs of the material after SPT at 400 °C under a strain rate of 2.7×10^{-1} s^{-1}: **a** deformation area and adjacent region, **b**, **c** deformation area and **d** die area.
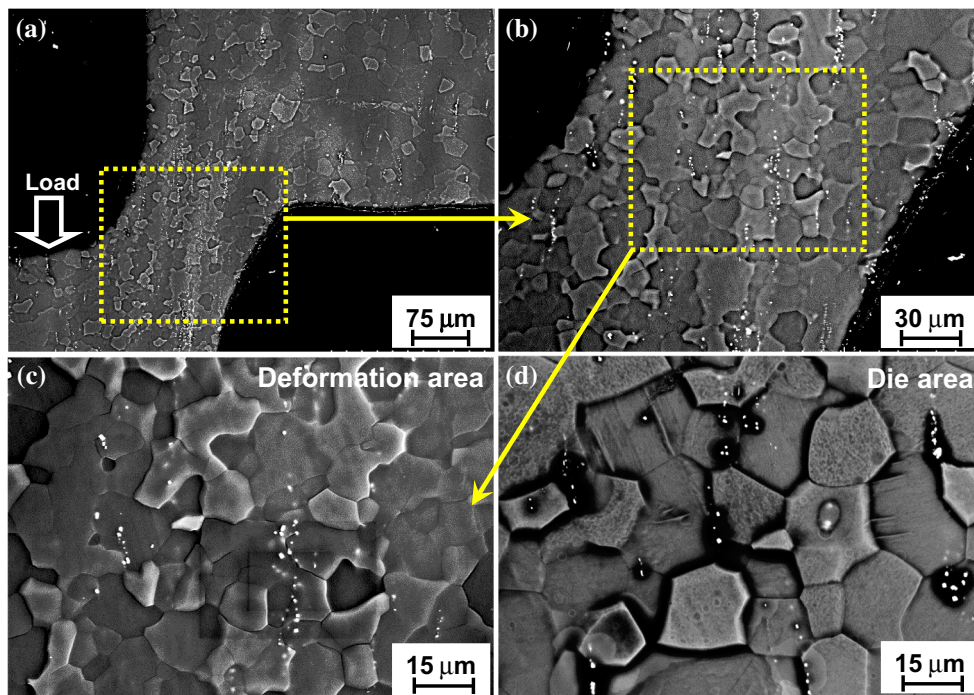
Figure 12 SEM micrographs of the material after SPT at 450 °C under a strain rate of 3.3×10^{-2} s^{-1}: **a** deformation area and adjacent regions, **b**, **c** deformation area and **d** die area.
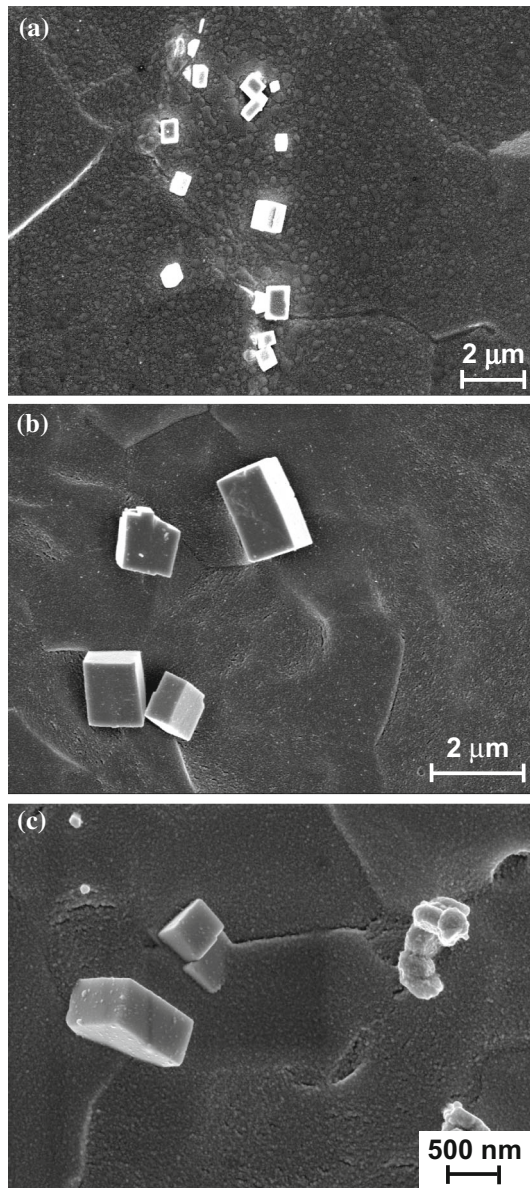
Figure 13 SEM micrographs of the material after SPT at 450 °C under a strain rate of 2.7×10^{-1} s^{-1}: **a, b** deformation area and adjacent regions, **c** deformation area and **d** die area.

presence of recrystallized grains in the microstructure of an Mg–Gd alloy at this temperature [32]. Accordingly, it is concluded that 350 °C is the temperature for the onset of recrystallization in the present Mg–Gd–Y–Zr alloy as observed in Fig. 10.

The higher onset temperature for the RE-containing alloys is due to the relative activity of different deformation systems in RE-containing alloys which is different from magnesium alloys without RE elements. Thus, the RE elements usually segregate at grain boundaries [14, 34, 35] and dislocations [36], dissolve in the Mg matrix and/or form clusters in the interiors of the grains [37] in addition to forming RE-rich particles. Accordingly, due to the low diffusion rates of these elements in magnesium, the RE elements may retard recrystallization so that higher temperatures are required for the onset of recrystallization in RE-containing Mg alloys. In this respect,

the diffusion coefficients of Y and Gd in Mg are similar, but they are almost one order of magnitude lower than for Al and Zn which are the conventional alloying elements in magnesium [38, 39].

In addition to DRX, another important feature of the microstructure of the Mg–5Gd–4Y–0.4Zr alloy after hot shear deformation is the stability of the Gd-rich and Y-rich cuboid particles at high deformation temperatures which serves to enhance the high-temperature strength of these alloys. The results in this investigation show there is no deformation, coarsening or fragmentation of these particles during hot shear deformation, and additionally, it seems that the dominant recrystallization mechanism of the material in the experimental temperature range is DDRX. Thus, there is no evidence for particle-stimulated nucleation (PSN) since no newly formed grains were formed around the cuboid particles.

Figure 14 Representative high-magnification FEGSEM micrographs of the material in the deformation area showing the morphologies of *cuboid* particles after hot shear deformation at 400 °C.

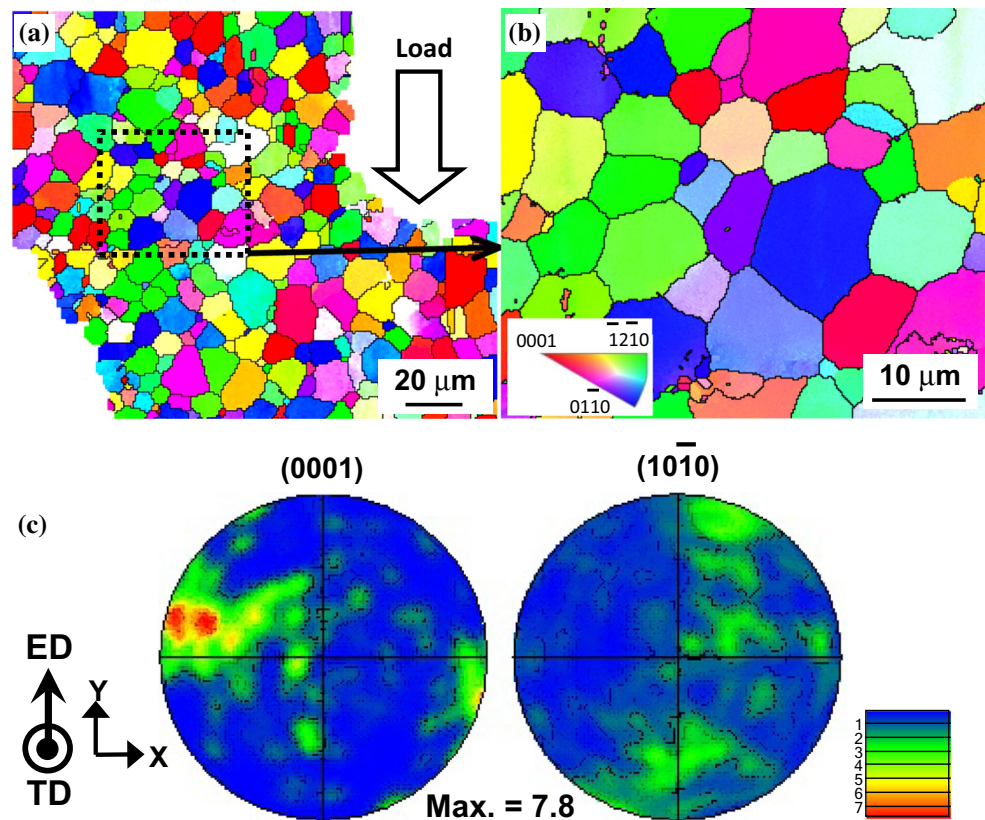## Textural evolution after hot shear deformation

In addition to the shape and size of the grains, the occurrence of DRX may also alter the crystallographic orientation of the grains and this determines the dominant texture of the material. Accordingly, the texture of the alloy was studied after hot shear deformation at 450 °C (Fig. 15) and it is now valuable to compare this result with the initial texture before SPT. The texture of the extruded Mg–5Gd–4Y–0.4Zr alloy before SPT was discussed in detail in an earlier report [14], and thus, it is described only briefly for comparison purposes.

It was shown earlier [14] that the texture of the extruded Mg–5Gd–4Y–0.4Zr alloy is different from RE-free Mg alloys wherein the basal planes are aligned parallel to the extrusion direction. In practice, the basal planes of the Mg–5Gd–4Y–0.4Zr alloy show an almost fibrous texture with an angle of about 60° between the ED and the normal vector of the basal planes. Therefore, this state can be considered as the initial texture of the material before SPT. After SPT at high temperatures, it is expected that the dominant texture is again a basal texture where basal planes are aligned in the direction of material flow in the sheared area due to the applied mechanical strain within the deformation area. However, the texture of the material in Fig. 15 is different and shows similarities to the trends reported earlier for the extruded alloy [14]. Thus, the dynamically recrystallized grains show a strong non-fibrous basal texture with a maximum intensity of 7.8 MRD. The preferred orientation of the basal planes is such that the angle between the normal direction and the transverse direction is about $-75°$ on the X axis and about 10° on the Y axis. This contrasts with the general behavior of RE-free Mg alloys where the deformation and recrystallization textures are similar [40]. It is concluded, therefore, that the RE elements alter the DRX texture after hot shear deformation where this is similar to results reported earlier for other modes of deformation such as hot extrusion [14] and hot compression [32, 33]. This difference is attributed to the segregation of RE elements at the grain boundaries and dislocation cores and also to the slow diffusivity of Gd and Y in Mg where these elements impede the movement of dislocations and grain boundaries through a solute drag effect [14].

Figure 15 **a**, **b** EBSD orientation maps and **c** pole figures after SPT at 450 °C under a strain rate of 3.3×10^{-2} s^{-1}.

Conclusions

The microstructural and textural evolutions of an extruded Mg–5Gd–4Y–0.4Zr alloy were evaluated after hot shear deformation by shear punch testing in the temperature range of 350–450 °C, and the following results were achieved:

1. The DRX starts at the grain boundaries of the deformed original grains and produces necklace-like structures at low deformation temperatures, thereby demonstrating discontinuous dynamic recrystallization as the dominant restoration process during hot shear deformation.

2. While the original grains were not recrystallized after deformation at 350 °C, some non-recrystallized deformed grains were detected in the microstructure of the material after SPT at 400 °C. By further increasing the SPT temperature to 450 °C, a fully recrystallized microstructure was obtained with well-defined equiaxed grains.

3. The Gd-rich and Y-rich cuboid particles retained their original shapes and sizes after hot shear deformation. No cracks, voids or fragmentation was observed around these particles. The stability of these particles and their compatibility with the Mg matrix are important parameters in enhancing the high-temperature strength of Mg–Gd–Y alloys.

4. EBSD orientation maps demonstrate a fully recrystallized microstructure after SPT at 450 °C with a non-fibrous basal DRX texture which is different from the conventional deformation texture.

References

[1] Boehlert CJ (2007) The tensile and creep behavior of Mg–Zn alloys with and without Y and Zr as ternary elements. J Mater Sci 42:3675–3684. doi:10.1007/s10853-006-1352-5

[2] Ning ZL, Wang GJ, Cao FY, Sun JF, Du JF (2009) Tensile deformation of a Mg–2.54Nd–0.26Zn–0.32Zr alloy at elevated temperature. J Mater Sci 44:4264–4269. doi:10.1007/s10853-009-3620-7

[3] Mahmudi R, Kabirian F, Nematollahi Z (2011) Microstructural stability and high-temperature mechanical properties of AZ91 and AZ91 + 2RE magnesium alloys. Mater Des 32:2583–2589

[4] Alizadeh R, Mahmudi R, Ngan AHW, Langdon TG (2015) Microstructural stability and grain growth kinetics in an extruded fine-grained Mg–Gd–Y–Zr alloy. J Mater Sci 50:4940–4951. doi:10.1007/s10853-015-9041-x

[5] Yao-Bo H, Deng J, Zhao C, Pan F-S, Peng J (2011) Microstructure and mechanical properties of Mg–Gd–Zr alloys with low gadolinium contents. J Mater Sci 46:5838–5846. doi:10.1007/s10853-011-5540-6

[6] Movahedi-Rad A, Mahmudi R (2014) Effect of Ag addition on the elevated-temperature mechanical properties of an extruded high strength Mg–Gd–Y–Zr alloy. Mater Sci Eng A 614:62–66

[7] Wang C, Guohua W, Lavernia EJ, Ding W (2017) Influences of heat treatment on microstructural evolution and tensile behavior of squeeze-cast Mg–Gd–Y–Zr alloy. J Mater Sci 52:1831–1846. doi:10.1007/s10853-016-0473-8

[8] Mordike BL (2002) Creep resistant magnesium alloys. Mater Sci Eng A 324:103–112

[9] Yin DD, Wang QD, Boehlert CJ, Ding WJ (2012) Creep and fracture behavior of as-cast Mg–11Y–5Gd–2Zn–0.5Zr (wt%). J Mater Sci 47:6263–6275. doi:10.1007/s10853-012-6546-4

[10] Alizadeh R, Mahmudi R, Langdon TG (2014) Superplasticity of a fine-grained Mg–9Gd–4Y–0.4Zr alloy evaluated using shear punch testing. J Mater Res Technol 3:228–232

[11] Alizadeh R, Mahmudi R, Ngan AHW, Huang Y, Langdon TG (2016) Microstructure, texture and superplasticity of a fine-grained Mg–Gd–Zr alloy processed by equal-channel angular pressing. Metall Mater Trans 47A:6056–6069

[12] Alizadeh R, Mahmudi R, Ngan AHW, Huang Y, Langdon TGL (2016) Superplasticity of a nano-grained Mg–Gd–Y–Zr alloy processed by high-pressure torsion. Mater Sci Eng A 561:786–794

[13] Alizadeh R, Mahmudi R, Pereira PHR, Huang Y, Langdon TG (2017) Microstructural evolution and superplasticity in an Mg–Gd–Y–Zr alloy after processing by different SPD techniques. Mater Sci Eng A 682:577–585

[14] Alizadeh R, Mahmudi R, Ngan AHW, Langdon TG (2016) An unusual extrusion texture in Mg–Gd–Y–Zr alloys. Adv Eng Mater 18:1044–1049

[15] Imandoust A, Barrett CD, Al-Samman T, Inal KA, El Kadiri H (2017) A review on the effect of rare-earth elements on texture evolution during processing of magnesium alloys. J Mater Sci 52:1–29. doi:10.1007/s10853-016-0371-0

[16] Ma ML, Zhang K, Li XG (2008) Hot deformation behavior of rare earth magnesium alloy without pre-homogenization treatment. Trans Nonferrous Met China 18:132–139

[17] Chen B, Zhou WM, Li S, Li XL, Lu C (2013) Hot compression deformation behavior and processing maps of Mg–Gd–Y–Zr alloy. J Mater Eng Perform 22:2458–2466

[18] Xia X, Chen Q, Zhang K, Zhao Z, Ma M, Li X, Li Y (2013) Hot deformation behavior and processing map of coarse-grained Mg–Gd–Y–Nd–Zr alloy. Mater Sci Eng A 587:283–290

[19] Xia X, Chen Q, Li J, Shu D, Hu C, Huang S, Zhao Z (2014) Characterization of hot deformation behavior of as-extruded Mg–Gd–Y–Zn–Zr alloy. J Alloys Compd 610:203–211

[20] Lu G, Xie Z, Zhang Z, Yang Y, Li B (2014) Hot compression deformation behavior of Mg–Gd–Y–Zn–Zr alloy. Appl Mech Mater 680:15–22

[21] Karami M, Mahmudi R (2012) Hot shear deformation constitutive analysis of an extruded Mg–6Li–1Zn alloy. Mater Lett 81:235–238

[22] Karami M, Mahmudi R (2014) Hot shear deformation constitutive analysis and processing map of extruded Mg–12Li–1Zn bcc alloy. Mater Des 53:534–539

[23] Sarebanzadeh M, Mahmudi R, Roumina R (2015) Constitutive analysis and processing map of an extruded Mg–3Gd–1Zn alloy under hot shear deformation. Mater Sci Eng A637:155–161

[24] Alizadeh R, Mahmudi R (2011) Effects of Sb addition on the modification of Mg_2Si particles and high-temperature mechanical properties of cast Mg–4Zn–2Si alloy. J Alloys Compd 509:9195–9199

[25] Mahmudi R, Alizadeh R, Azhari S (2013) Strain rate sensitivity of equal-channel angularly pressed Sn–5Sb alloy determined by shear punch test. Mater Lett 97:44–46

[26] Hankin GL, Toloczko MB, Johnson KI, Khaleel MA, Hamilton ML, Garner FA, Davies RW, Faulkner RG (2000) Improvement of post irradiation ductility of V–Ti–Cr–Si type alloys neutron irradiated around 400C. ASTM STP 1366:1018–1028

[27] Park WJ, Park H, Kim DH, Kim NJ (1994) Structure and decomposition behavior of rapidly solidified Mg–Nd–X (X = Al, Si) alloys. Mater Sci Eng A179–180:637–640

[28] Vostry P, Smola B, Stulikova I, Von Buch F, Mordike BL (1999) Microstructure evolution in isochronally heat treated Mg–Gd alloys. Phys Stat Solidi 175A:491–500

[29] Li D, Wang Q, Ding W (2006) Characterization of phases in Mg–4Y–4Sm–0.5Zr alloy processed by heat treatment. Mater Sci Eng A 428:295–300

[30] He SM, Zeng XQ, Peng LM, Gao X, Nie JF, Ding WJ (2007) Microstructure and strengthening mechanism of high strength Mg–10Gd–2Y–0.5Zr alloy. J Alloy Compd 427:316–323

[31] Yang Z, Wang ZH, Duan HB, Guo YC, Gao PH, Li LP (2015) Microstructure evolution of Mg–6Gd–2Y alloy during solid solution and aging process. Mater Sci Eng A 631:160–165

[32] Stanford N, Callaghan MD, de Jong B (2013) The effect of rare earth elements on the behaviour of magnesium-based alloys: Part 1—Hot deformation behavior. Mater Sci Eng A 565:459–468

[33] Stanford N (2013) The effect of rare earth elements on the behaviour of magnesium-based alloys: Part 2—recrystallisation and texture development. Mater Sci Eng A 565:469–475

[34] Stanford N, Atwell D, Barnett MR (2010) The effect of Gd on the recrystallisation, texture and deformation behaviour of magnesium-based alloys. Acta Mater 58:6773–6783

[35] Stanford N, Sha G, Xia JH, Ringer SP, Barnett MR (2011) Solute segregation and texture modification in an extruded magnesium alloy containing gadolinium. Scr Mater 65:919–921

[36] Stanford N, Sabirov I, Sha G, LaFontaine A, Ringer SP, Barnett MR (2010) Effect of Al and Gd solutes on the strain rate sensitivity of magnesium alloys. Metall Mater Trans 41A:734–743

[37] Stanford N, Sha G, La Fontaine A, Barnett MR, Ringer SP (2009) Atom probe tomography of solute distributions in Mg-based alloys. Metall Mater Trans 40A:2480–2487

[38] Das SK, Kim YM, Ha TK, Gauvin R, Jung IH (2013) Anisotropic diffusion behavior of Al in Mg: diffusion couple study using Mg single crystal. Metall Mater Trans 44A:2539–2547

[39] Das SK, Kang YB, Ha T (2014) Thermodynamic modeling and diffusion kinetic experiments of binary Mg–Gd and Mg–Y systems. Acta Mater 71:164–175

[40] Al-Samman T, Gottstein G (2008) Dynamic recrystallization during high temperature deformation of magnesium. Mater Sci Eng A 490:411–420